Taylor & Francis
Taylor & Francis Group

Vehicle System Dynamics

International Journal of Vehicle Mechanics and Mobility

ISSN: 0042-3114 (Print) 1744-5159 (Online) Journal homepage: http://www.tandfonline.com/loi/nvsd20

Design of passive vehicle suspensions for maximal least damping ratio

Malcolm C. Smith & Stuart J. Swift

To cite this article: Malcolm C. Smith & Stuart J. Swift (2016) Design of passive vehicle suspensions for maximal least damping ratio, Vehicle System Dynamics, 54:5, 568-584, DOI: 10.1080/00423114.2016.1145242

To link to this article: http://dx.doi.org/10.1080/00423114.2016.1145242

VEHICLE SYSTEM DYNAMICS, 2016
VOL. 54, NO. 5, 568–584
http://dx.doi.org/10.1080/00423114.2016.1145242

Design of passive vehicle suspensions for maximal least damping ratio

Malcolm C. Smith and Stuart J. Swift

Department of Engineering, University of Cambridge, Cambridge, UK

ABSTRACT

This paper studies the use of the least damping ratio among system poles as a performance metric in passive vehicle suspensions. Methods are developed which allow optimal solutions to be computed in terms of non-dimensional quantities in a quarter-car vehicle model. Solutions are provided in graphical form for convenient use across vehicle types. Three suspension arrangements are studied: the standard suspension involving a parallel spring and damper and two further suspension arrangements involving an inerter. The key parameters for the optimal solutions are the ratios of unsprung mass to sprung mass and suspension static stiffness to tyre vertical stiffness. A discussion is provided of performance trends in terms of the key parameters. A comparison is made with the optimisation of ride comfort and tyre grip metrics for various vehicle types.

ARTICLE HISTORY
Received 1 October 2015
Revised 10 January 2016
Accepted 16 January 2016

KEYWORDS
Suspension systems; passive suspensions; damping ratio; inerter

1. Introduction

Analytical solutions for optimal suspensions provide guidance not only on parameter settings, but more importantly, have the potential to offer insight into vehicle design. In particular, the dependence of an optimum on key parameters or ratios can influence design at the vehicle concept stage before a suspension system is conceived or optimised. Such information is especially useful if design choices are being considered that lie outside the parameter ranges of traditional designs.

The results of the present paper complement those presented in [1] which derived analytical solutions for ride comfort and grip for some simple passive network structures. Here we consider a less common metric for vehicle suspensions—the least damping ratio among system poles. In comparison to other measures, such as those related to comfort, grip, and handling, it is more generic. Nevertheless, the extent of oscillatory behaviour exhibited by the system can still be considered as a fundamental and important property in vehicle performance. As such an understanding of how this measure can be improved or maximised has the potential to provide useful insight into suspension system design. It should be mentioned that examples of the use of least damping ratio can be found in the literature on vehicle suspensions. See, for example, [2] for a discussion on the best value of damping ratio in relation to other vehicle performance metrics for a roll plane model of

CONTACT Malcolm C. Smith mcs@eng.cam.ac.uk

a heavy truck. In [3] the least damping ratio has been used in the characterisation of a 'road-friendly' suspension for European trucks. In [4, p.824] specific values for optimum damping ratios have been proposed in the context of racing cars.

The present paper provides optimal solutions for the least damping ratio in terms of non-dimensional quantities. A quarter-car vehicle model is used for the study together with three suspension networks comprising a damper, parallel damper-inerter and series damper-inerter in parallel with the main spring. Using root-locus ideas, a necessary and sufficient condition is derived for all system poles to be on the negative real axis, for some choice of damping parameter, when all other parameters are fixed. The condition is shown to depend upon two critical frequencies. For the first suspension arrangement these frequencies are functions of just two ratios: $m_u/m_s, k_s/k_t$ where m_u, m_s, k_s, k_t are the unsprung and sprung masses, suspension static stiffness and tyre vertical stiffness. A further ratio involving the inertance comes into play for the second and third suspension arrangements. For the suspension networks considered, this paper computes the maximal least damping ratio as a function of damping (for the first network) and as a function of damping and inertance (for the second and third networks). Contour plots are provided in terms of the two fundamental ratios. Optimal parameters (suitably normalised) are expressed in the same manner. A comparison is made for a range of vehicle types with the optimisation of ride comfort and tyre grip metrics.

2. Preliminaries

We will consider the standard quarter-car model of Figure 1 consisting of the sprung mass m_s , the unsprung mass m_u and the tyre vertical stiffness k_t. The suspension strut provides an equal and opposite force on the sprung and unsprung mass and is assumed here to be a passive mechanical admittance $Y(s)$ (defined by the ratio of Laplace transformed force to relative velocity). The model has the characteristic equation:

$$s^4 m_u m_s + s^3 Y(m_u + m_s) + s^2 m_s k_t + s Y k_t = 0. \tag{1}$$

We will consider the suspension networks shown in Figure 2, according to the numbering of Scheibe and Smith,[1] which make use of the inerter device introduced in [5]. The

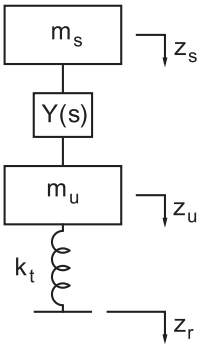

Figure 1. Quarter-car diagram.

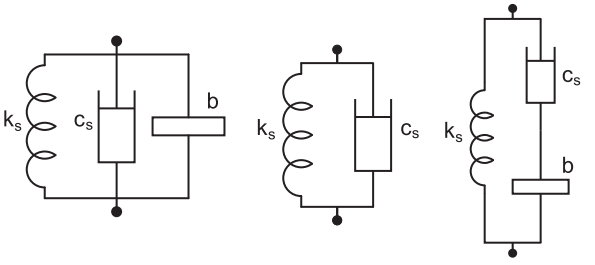

Figure 2. Suspension networks S1, S3 and S4.

suspension admittance $Y(s)$ for network S3 is

$$sY = bs^2 + c_s s + k_s$$

and the suspension admittance for network S4 is

$$sY = \frac{s^2 c_s b + s k_s b + k_s c_s}{c_s + sb} = \frac{s^2 + s k_s {c_s}^{-1} + k_s b^{-1}}{s {c_s}^{-1} + b^{-1}}.$$

With the assumption that m_u, m_s , k_s, k_t, $c_s, b > 0$, the roots of the characteristic Equation (1) all have negative real parts. For any complex conjugate pair of roots, there is a corresponding quadratic factor $s^2 + 2\zeta\omega_n s + \omega_n^2$ where ζ $(0 < \zeta < 1)$ is called the damping ratio and ω_n (> 0) the undamped natural frequency. We define the least damping ratio J_ϕ to be the smallest ζ among all the complex conjugate pairs of roots of Equation (1). If all the roots of Equation (1) are real (and negative) then we set $J_\phi = 1$. We note that this differs from the treatment of purely second-order systems for which values of ζ greater than one are termed overdamped systems. We note that increasing J_ϕ corresponds to reducing oscillations in the system, which is our motivation for maximising this measure.

We introduce the following dimensionless parameters:

$$\alpha = m_\mathrm{u}/m_\mathrm{s}, \tag{2}$$

$$\beta = k_s/k_t, \tag{3}$$

$$\gamma = \delta^{-1} = b/m_\mathrm{s}, \tag{4}$$

$$c = \frac{c_s}{\sqrt{k_t(m_\mathrm{u} + m_\mathrm{s})}}. \tag{5}$$

We will make use of γ (resp. δ) when considering the S3 (resp. S4) network since this reduces to S1 when $\gamma = 0$ (resp. $\delta = 0$).

3. Root-locus analysis and the critical frequencies ω_1, ω_2

Insight into the nature of the problem of maximising least damping ratio is provided by a root locus analysis and the introduction of a pair of critical frequencies. We consider first the quarter car with suspension admittance S3 (which includes S1 as a special case). After

rearrangement the characteristic equation can be written in the form

$$(m_u m_s + b(m_u + m_s))s^4 + (k_s(m_u + m_s) + k_t(b + m_s))s^2 + k_t k_s + c_s s((m_u + m_s)s^2 + k_t) = 0. \quad (6)$$

This form allows an investigation using root loci with c_s as the variable parameter.

Proposition 1: *The characteristic Equation* (6) *always reduces to*

$$(s^2 + {\zeta_1}^2)(s^2 + {\zeta_2}^2) + c_s s\left(\frac{m_u + m_s}{m_u m_s + b(m_u + m_s)}\right)\left(s^2 + \frac{k_t}{m_u + m_s}\right) = 0, \quad (7)$$

where ζ_1, ζ_2 *are real and satisfy*

$${\zeta_1}^2 < \frac{k_t}{m_u + m_s} < {\zeta_2}^2. \quad (8)$$

Proof: With the substitution $\lambda = s^2$ the terms in Equation (6) that are independent of c_s reduce to a quadratic in λ. It can be checked directly that this quadratic has a positive discriminant and further that its roots are real, distinct and negative, and hence may be denoted as $-\zeta_1^2, -\zeta_2^2$. It can further be verified directly that the quadratic is negative when $\lambda = -k_t/(m_u + m_s)$ from which Equation (8) follows. ■

Accordingly we can place the root-locus zeros (terminal locations as $c_s \to \infty$) at $\pm j$ using the frequency scaling

$$s \to s\sqrt{\frac{k_t}{m_u + m_s}}, \quad (9)$$

whereupon Equation (7) reduces to

$$(s^2 + {\omega_1}^2)(s^2 + {\omega_2}^2) + c_0 s(s^2 + 1) = 0, \quad (10)$$

where $0 < {\omega_1}^2 < 1, 1 < {\omega_2}^2$ and

$$c_0 = c\frac{(1 + \alpha)^2}{\alpha + \gamma + \alpha\gamma}$$

with the non-dimensional damping parameter c being defined in (5). The critical frequencies ω_1, ω_2 expressed as a function of non-dimensional quantities are given by

$${\omega_1}^2, {\omega_2}^2 = \frac{1 + \alpha}{2(\alpha + \gamma + \alpha\gamma)}\left(\beta(1 + \alpha) + (1 + \gamma) \mp \sqrt{\left(\beta(1 + \alpha) + (1 + \gamma)\right)^2 - 4\beta(\alpha + \gamma + \alpha\gamma)}\right). \quad (11)$$

It should be noted that the frequency scaling (9) leaves the damping ratios of the roots of Equation (6) unaffected, and hence equal to those of Equation (10).

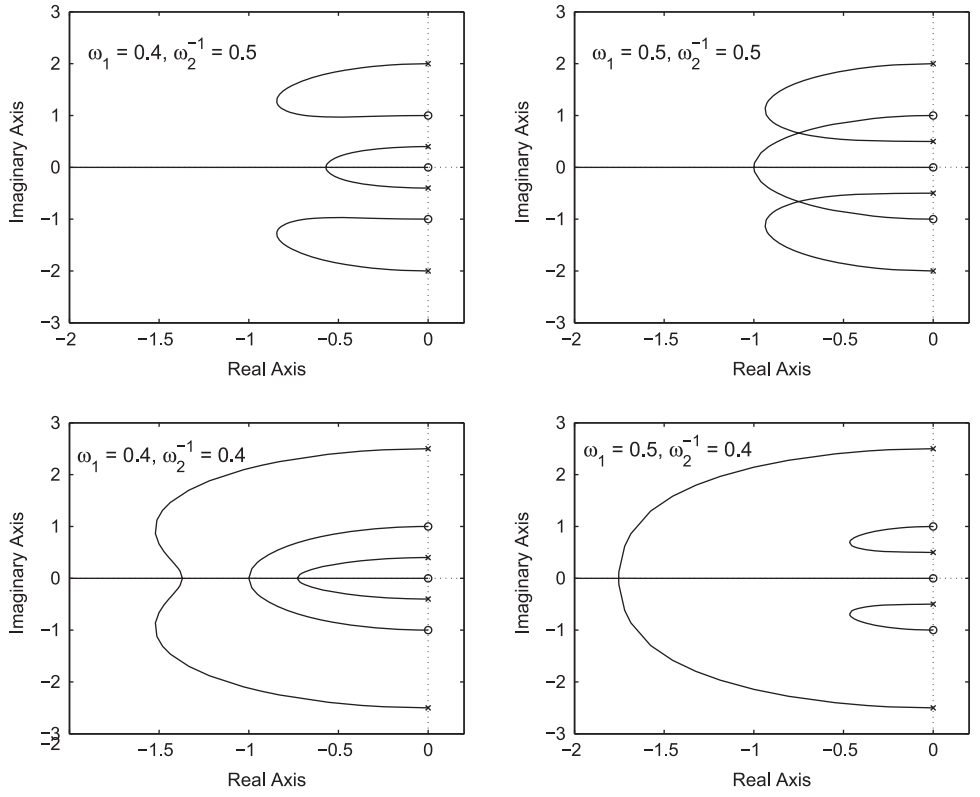

Figure 3. Root-locus examples for values of ω_1, ω_2.

The general form of the root-locus diagram for Equation (10) depends upon the values of the critical frequencies, as illustrated in Figure 3. For the first, second and fourth cases it is clear that no choice of c_s allows all four roots to be real. An interesting special case is shown in the second sub-figure where the maximal least damping ratio results in coincident complex conjugate roots. Only in the third case do there exist choices of c_s for which all four roots are real.

For any given ω_1, ω_2 we consider the problem of maximising J_ϕ as a function of c_0 for Equation (10). The contours of optimal J_ϕ were calculated using numerical techniques and are shown in Figure 4. Several complementary techniques (Differential Evolution, Genetic Algorithm, Particle Swarm Optimisation, Simulated Annealing) were used in an effort to ensure that global optima were found.

It can be seen that Figure 4 is symmetrical under the transformation $\omega_1 \longleftrightarrow {\omega_2}^{-1}$. This can be verified by considering the mapping $s \longleftrightarrow s^{-1}$ in Equation (10) which inverts the magnitude of a pair of complex poles whilst preserving the damping ratio. Under this mapping the characteristic Equation (10) becomes

$$(s^2 + {\omega_2}^{-2})(s^2 + {\omega_1}^{-2}) + \frac{c_0 s(s^2+1)}{{\omega_1}^2 {\omega_2}^2} = 0, \tag{12}$$

which is then identitical with Equation (10) after the substitution $\omega_1 \to \omega_2^{-1}$ (apart from a rescaling of c_0).

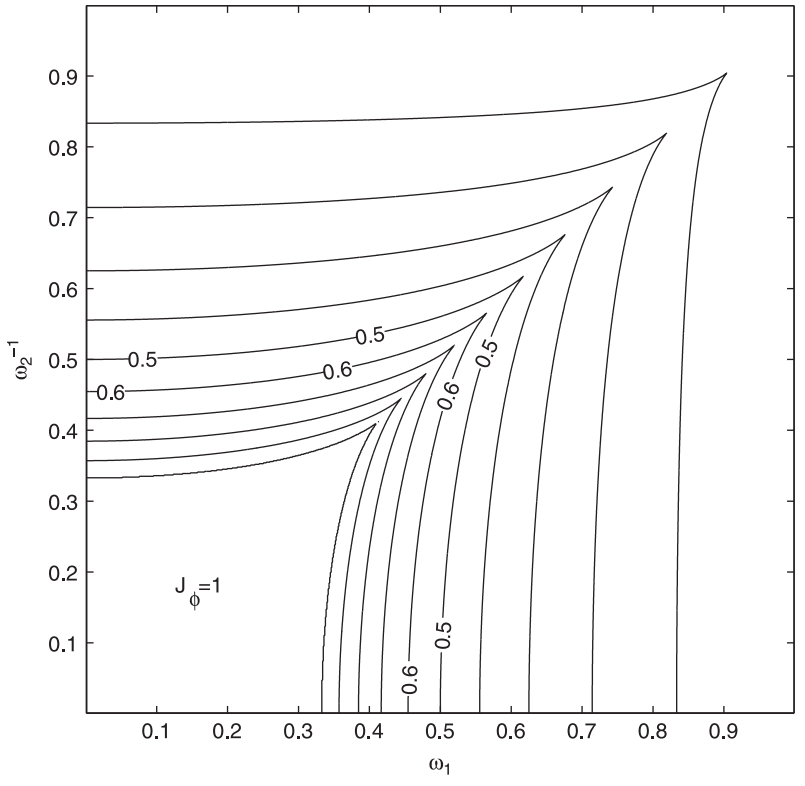

Figure 4. Contours of optimal J_ϕ as a function of ω_1, ω_2 for Equation (10).

It can be seen that there is a region in Figure 4 where $J_\phi = 1$ can be achieved. The boundary curves for this region can be found analytically as follows.

Theorem 1: *There exists* $c_0 > 0$ *such that the quartic* (10) *has all roots real and negative if and only if*

$$4{a_1}^3 - {a_2}^2{a_1}^2 - 18a_0a_2a_1 + 4a_0{a_2}^3 + 27{a_0}^2 < 0,$$

where

$$\begin{aligned} a_0 &= -{\omega_1}^2{\omega_2}^2, \\ a_1 &= {\omega_1}^2 + {\omega_2}^2 - 3{\omega_1}^2{\omega_2}^2, \\ a_2 &= 3 - {\omega_1}^2 - {\omega_2}^2. \end{aligned}$$

Proof: The breakaway points of the root locus are given by the roots of

$$s^6 + s^4(3 - {\omega_1}^2 - {\omega_2}^2) + s^2({\omega_1}^2 + {\omega_2}^2 - 3{\omega_1}^2{\omega_2}^2) - {\omega_1}^2{\omega_2}^2 = 0. \tag{13}$$

(The LHS of Equation (13) equals $nm' - n'm$ when we write Equation (10) in the form $m(s) + c_0 n(s) = 0$.)

For c_0 small and positive there must be four complex roots of Equation (10) and for c_0 sufficiently large and positive there must be two complex roots and two real roots. Hence,

the only possibility for the existence of a $c_0 > 0$ such that Equation (10) has all roots real and negative is that there are three real negative roots of Equation (13). Given that the roots of Equation (13) are symmetric with respect to the imaginary axis this is equivalent to

$$f(x) = x^3 + a_2x^2 + a_1x + a_0$$

having three real positive roots. Define $f_1(x) = f(x)$, $f_2(x) = f'(x)$, $-f_3(x)$ equal to the remainder on dividing $f_1(x)$ by $f_2(x)$, and $-f_4$ equal to the remainder on dividing $f_2(x)$ by $f_3(x)$. We can calculate that

$$\begin{aligned} f_2(x) &= 3x^2 + 2a_2x + a_1, \\ f_3(x) &= -(2/3a_1 - 2/9{a_2}^2)x + 1/9a_2a_1 - a_0, \\ f_4 &= -9/4\frac{4{a_1}^3 - {a_2}^2{a_1}^2 - 18a_0a_2a_1 + 4a_0{a_2}^3 + 27{a_0}^2}{({a_2}^2 - 3a_1)^2}. \end{aligned}$$

The sequence $f_1, \ldots, f_4$ is a Sturm chain [6] with the property that the number of distinct real roots of $f(x)$ in the interval $(0, \infty)$ is equal to $V(0) - V(\infty)$ where $V(0)$ and $V(\infty)$ are the number of sign changes in the chain functions evaluated at $x = 0$ and $x = \infty$, respectively. Hence for three real roots we require $V(0) - V(\infty) = 3$. As the chains only have four functions, f_1 to f_4, we require three sign changes in the functions evaluated at zero and no sign changes when they are evaluated at infinity where we interpret $f_i(\infty)$ to be the coefficient of the highest power of x in $f_i(x)$. Observing that $f_1(0) = -{\omega_1}^2{\omega_2}^2$ is always negative and $f_1(\infty) > 0$ the required signs must be as given in Table 1. These conditions further reduce to $f_2(0) > 0, f_3(0) < 0, f_3(\infty) > 0$ and $f_4 > 0$, which can be expressed as

$$\begin{aligned} a_1 &> 0, \\ a_1a_2 - 9a_0 &< 0, \\ {a_2}^2 - 3a_1 &> 0, \\ 4{a_1}^3 - {a_2}^2{a_1}^2 - 18a_0a_2a_1 + 4a_0{a_2}^3 + 27{a_0}^2 &< 0. \end{aligned}$$

Writing in terms of ω_1, ω_2 these become

$$\begin{aligned} &{\omega_1}^{-2} + {\omega_2}^{-2} - 3 > 0, \\ &\quad -{\omega_1}^4 - {\omega_2}^4 + 3{\omega_1}^4{\omega_2}^2 + 3{\omega_2}^4{\omega_1}^2 - 2{\omega_1}^2{\omega_2}^2 + 3{\omega_1}^2 + 3{\omega_2}^2 > 0, \\ &{\omega_1}^4 + {\omega_2}^4 - 9{\omega_1}^2 - 9{\omega_2}^2 + 11{\omega_1}^2{\omega_2}^2 + 9 > 0, \end{aligned}$$

Table 1. Sturm chain signs required for three real roots of $f(x)$.

	$x = 0$	$x = \infty$
$f_1(x)$	$-$	$+$
$f_2(x)$	$+$	$+$
$f_3(x)$	$-$	$+$
f_4	$+$	$+$

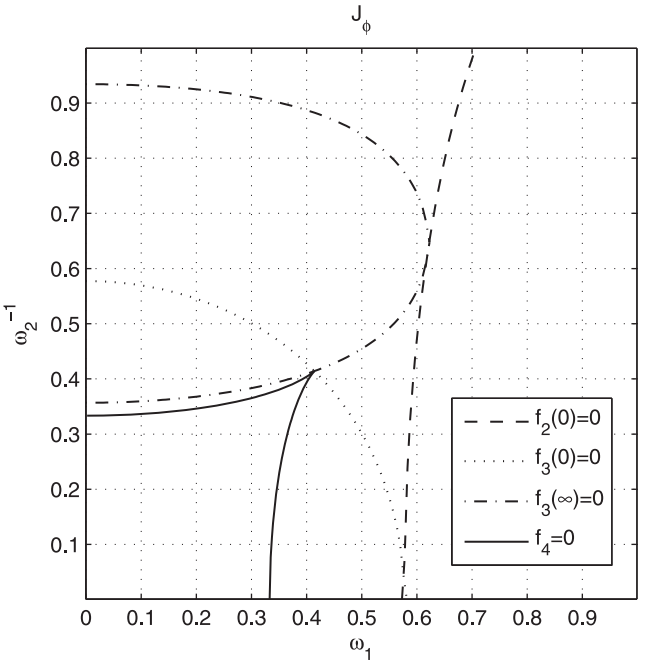

Figure 5. Sturm chain conditions.

$$(\omega_2{}^2 - 1)(\omega_1{}^2 - 1)(-\omega_1{}^6\omega_2{}^6 + 9\omega_1{}^6\omega_2{}^2 + 9\omega_1{}^2\omega_2{}^6 + 126\omega_1{}^4\omega_2{}^4 + 126\omega_1{}^2\omega_2{}^2 - 111\omega_1{}^4\omega_2{}^2 - 111\omega_2{}^4\omega_1{}^2 + 9\omega_1{}^4 + 9\omega_2{}^4) > 0.$$

The conditions for equality are shown in Figure 5 for $0 < \omega_1, \omega_2 < 1$. By finding the resultant of f_4 with $f_3(0)$ and $f_3(\infty)$ we can check that $f_4 = 0$ intersects $f_3(0) = 0$ and $f_3(\infty) = 0$ only at the point

$$\omega_1 = \omega_2{}^{-1} = \sqrt{2} - 1$$

in the region $0 < \omega_1, \omega_2^{-1} < 1$. It can then be seen from Figure 5 that if the $f_4 > 0$ condition is satisfied then all the other inequalities are also satisfied.

■

4. Contours of maximal least damping ratio in terms of non-dimensional parameters

4.1. Optimal J_ϕ for S1 and S3

We now compute contours of maximal J_ϕ and corresponding optimal parameters for the S1 and S3 networks in the non-dimensional parameters α and β as defined in Equations (2) and (3). As in the computations of Section 3 numerical techniques were deployed to search for the global optimum $\hat{J}_\phi$ as a function of suspension normalised damping c and normalised inertance γ. These calculations are performed point-wise over a fine grid in α and β. At values of α and β where $\hat{J}_\phi = 1$ there can be several values of damping c for which the optimum can be achieved. This can be understood from the root-locus plots

in Figure 3, which show that the roots may lie on the real axis for a range of values of c. Figure A1 provides the optimal solutions for J_ϕ for the S1 network, while Figures A2–A3 provide the optimal solutions for the S3 network (see appendix).

Regarding general trends it can be seen that, for small enough α and β, $\hat{J}_\phi = 1$. Above a certain threshold $\hat{J}_\phi$ decreases with increasing α or β. This agrees with the intuition that a suspension system becomes more oscillatory with increasing unsprung mass or increasing static suspension stiffness. A similar pattern of optimal least damping ratio is seen for S3, though with a percentage improvement over the S1 network for sufficiently large β. Note that the region $\hat{J}_\phi = 1$ extends to higher values of β and the percentage improvement over S1 improves with increasing β. Within the region $\hat{J}_\phi = 1$ there is some choice over the values of damper rate c and inertance b. The contours shown are the solutions that achieve $\hat{J}_\phi = 1$ with the smallest value of damper rate.

Remark 1: There appears to be an explicit formula for optimal inertance for S3 given by

$$\gamma = \frac{\beta(1+\alpha)^2 - \alpha}{1+\alpha} \tag{14}$$

for $\beta \geq \alpha/(1+\alpha)^2$ and providing the optimal $\hat{J}_\phi < 1$, and with the corresponding optimal damping being

$$c = \frac{(\alpha + \gamma(1+\alpha))}{(1+\alpha)^2} \frac{2(1-\omega_1^2)}{\omega_1}, \tag{15}$$

where ω_1^2 is defined in Equation (11). The evidence to support this comes from superimposing curves of $(\omega_1, \omega_2^{-1})$ as a function of γ, for fixed α and β, onto the plot of Figure 4, and observing that the maximum $\hat{J}_\phi$ occurs on the line $\omega_1 = \omega_2^{-1}$. For the latter condition the optimal c_0 causes (7) to have coincident roots. The expression (14) follows from Equation (11) by setting $\omega_1 = \omega_2^{-1}$, and Equation (15) follows by equating (10) with $(s^2 + ds + 1)^2$ for some $d > 0$.

Similar considerations apply to find the optimal β for fixed α for S1, to give the formula

$$\beta = \frac{\alpha}{(1+\alpha)^2}$$

for α large enough so that $\hat{J}_\phi < 1$.

4.2. Optimal J_ϕ for S4

Combining the quarter-car model with suspension admittance S4 and rearranging the characteristic equation gives

$$c_s(s^4(m_\mathrm{u} m_\mathrm{s} b^{-1} + (m_\mathrm{u} + m_\mathrm{s})) + s^2((m_\mathrm{u} + m_\mathrm{s})k_s b^{-1} + k_t(1 + m_\mathrm{s} b^{-1})) + k_t k_s b^{-1})$$
$$+ s(s^4 m_\mathrm{u} m_\mathrm{s} + s^2(k_s(m_\mathrm{u} + m_\mathrm{s}) + k_t m_\mathrm{s}) + k_t k_s) = 0,$$

which takes the form of a root-locus defining equation with c_s being the variable parameter. Applying a shift in s

$$s \to s\sqrt{\frac{k_t}{m_\mathrm{u} + m_\mathrm{s}}}$$

then gives, after some rearrangement,

$$c(1+\alpha)(s^4(1+\alpha+\alpha\delta)+s^2(1+\alpha)(1+\delta+\beta\delta+\alpha\beta\delta)+\beta\delta(1+\alpha)^2)$$
$$+s(s^4\alpha+s^2(1+\alpha)(1+\beta+\alpha\beta)+\beta(1+\alpha)^2)=0,$$

where α, β, δ and c are defined by Equations (2)–(5).

The maximal J_ϕ values are again computed point-wise over a fine grid. Figures A4–A5 (appendix) provide the optimal solutions for the S4 network. The main difference in the pattern of optimal least damping ratio for S4 is the increased range of values of β for which $\hat{J}_\phi = 1$. This region also extends to higher values of α than in the other networks. Increasing β further gives values of $\hat{J}_\phi$ which are similar to those for S3. It can be seen that the percentage improvement is always larger for S4 than S3.

5. Comparison with ride comfort and tyre grip metrics

In [1] optimal solutions for ride comfort and tyre grip were derived for the quarter-car model with metrics defined as follows:

$$J_1 = 2\pi\sqrt{V\kappa}\,\|s^{-1}T_{z_r\to\ddot{z}_s}(j\omega)\|_2,$$
$$J_3 = 2\pi\sqrt{V\kappa}\,\|s^{-1}T_{z_r\to k_t(z_u-z_r)}(j\omega)\|_2,$$

Table 2. Suspension parameters and optimal normalised damping for various vehicle types.[7,8]

Vehicle type		m_u (kg)	m_s (kg)	k_s (N/mm)	k_t (N/mm)	c_s bump (kNs/m)	c_s rebound (kNs/m)
C	Front	46	323	12.80	170	1.0	2.0
Coupe	Rear	60	264	13.80	150	0.8	1.4
D	Front	53	380	12.95	180	1.2	1.8
Saloon	Rear	44	337	14.72	170	1.0	1.8
F	Front	45	400	20.00	250	4.1	5.8
Sports	Rear	50	400	20.00	250	4.1	5.8
G	Front	23	125	300	228	6.0	10.0
F1car	Rear	30	188	200	228	11.0	15.0
H	Front	35	209	230	375	8.0	12.0
C1 prototype	Rear	45	301	400	398	12.0	16.0
Truck	Front	177	1872	232	1030	26.2	–
	Rear	277	1411	500	2060	34.7	

Vehicle type		α	β	Bump c(–)	Rebound c(–)	Optimal damping c (–) for J_ϕ	J_1	J_3	$\hat{J}_\phi$
C	Front	0.142	0.075	0.126	0.252	0.562	0.075	0.291	1.0
Coupe	Rear	0.227	0.092	0.101	0.177	0.588	0.092	0.322	0.818
D	Front	0.138	0.072	0.136	0.204	0.558	0.072	0.289	1.0
Saloon	Rear	0.163	0.087	0.113	0.204	0.579	0.087	0.300	1.0
F	Front	0.113	0.080	0.389	0.550	0.538	0.080	0.271	1.0
Sports	Rear	0.125	0.080	0.389	0.550	0.551	0.080	0.280	1.0
G	Front	0.184	1.316	1.033	1.722	1.768	1.316	1.223	0.130
F1car	Rear	0.160	0.775	1.894	2.582	1.268	0.775	0.720	0.220
H	Front	0.167	0.613	0.836	1.254	1.105	0.613	0.575	0.271
C1 prototype	Rear	0.150	1.005	1.254	1.672	1.502	1.005	0.939	0.175
Truck	Front	0.094	0.225	0.571	–	0.759	0.225	0.295	0.662
	Rear	0.196	0.243	0.755	–	0.735	0.243	0.327	0.615

where V is the vehicle velocity in m/s, κ is the road roughness in m/cycle, and $T_{x\to y}$ denotes the Laplace transfer function from x to y. These solutions are now compared to the optimisation of J_ϕ for the network S1 for a selection of typical vehicle parameters – see Table 2. It may be seen that the optimal damper value for J_ϕ is typically larger than that for J_3 which is in turn larger than for J_1.

The case of stiffly sprung vehicles is interesting to consider. Table 2 shows that the practical values of bump and rebound damping are typically closer to the J_ϕ value than those of J_3 and J_1. This suggests that the J_ϕ metric does behave sensibly when optimised alone as vehicle parameters become more extreme.

6. Concluding remarks

This paper has provided a solution to the problem of maximising the least damping ratio among system poles in a quarter-car vehicle suspension for three suspension networks. It has been shown that the solution can be expressed in terms of two ratios: unsprung mass to sprung mass $\alpha = m_{\mathrm{u}}/m_{\mathrm{s}}$ and suspension static stiffness to tyre vertical stiffness $\beta = k_s/k_t$. Results have been displayed in terms of contour plots on a grid of the dimensionless parameters.

Root-locus analysis has highlighted the importance of a pair of critical frequencies in determining the best achievable damping ratio. These critical frequencies are functions of the dimensionless parameters. The method of Sturm chains has characterised analytically the boundary curves which determine whether all the poles can be placed on the real axis (Theorem 1).

The contour plots allow easy evaluation of the benefits of the three simple suspension struts across a range of vehicle types. The contour plots show that both the S3 (parallel damper-inerter) and S4 (series damper-inerter) networks give an improvement over the conventional S1 network for β larger than around 0.15 (for a typical value of α). The region of the parameter space where improvement is possible is identical for S3 and S4, but larger percentage improvements can be obtained with S4. For the S1 network it was seen that the optimal damper value is typically larger than for the standard tyre grip metric, which is in turn typically larger than for a standard ride comfort metric, but with values tending to be closer for stiffly sprung vehicles. Contour plots for a larger range of α and β are given in [9].

Previous work that has made use of the damping ratio as a performance metric has already been mentioned.[2–4] Further work to understand the metric for half-car and full-car models is desirable. Here, we are content to point out that the stand-alone measure does show promise as a broad indicator of vehicle performance and that there is a case for it to be included more routinely as a metric in vehicle suspension design.

Disclosure statement

No potential conflict of interest was reported by the authors.

Funding

This work was supported by the Engineering and Physical Sciences Research Council grant numbers [EP/F062656/1] and [EP/G066477/1].

References

[1] Scheibe F, Smith MC. Analytical solutions for optimal ride comfort and tyre grip for passive vehicle suspensions. Veh Syst Dyn. 2009;47(10):1229–1252.
[2] Ahmadian M, Simon DE. An analytical and experimental evaluation of magneto-rheological suspensions for heavy trucks. Int J Veh Syst Dyn. 2002;37(IAVSD Suppl. 37):38–49.
[3] OECD. Performance-based standards for the road sector. Paris: OECD Publishing; 2005, ISBN 92-821-2337-5.
[4] Milliken WF, Milliken DL. Race car vehicle dynamics. SAE; 1995, page 824, ISBN 1-56091-526-9.
[5] Smith MC. Synthesis of mechanical networks: the inerter. IEEE Trans Autom Control. 2002;47(10):1648–1662.
[6] Gantmacher FR. The theory of matrices, Vol. II. New York: Chelsea; 1980, Chapter XV, Section 2.
[7] Dixon JC. Tyres, suspension and handling. Cambridge: Cambridge University Press; 1991, Appendix C, Table C.1.
[8] Kitching KJ, Cole DJ, Cebon D. Theoretical investigation into the use of controllable suspensions to minimize road damage. Proc Instit Mech Eng, Part D: J Autom Eng. 2000;214:13–31.
[9] Smith MC, Swift SJ. A parametric study of optimal passive suspensions for least damping ratio, comfort and grip. Technical Report: CUED/F-INFENG/TR.683, December 2012.

Appendix. Contour plots for $\hat{J}_\phi$

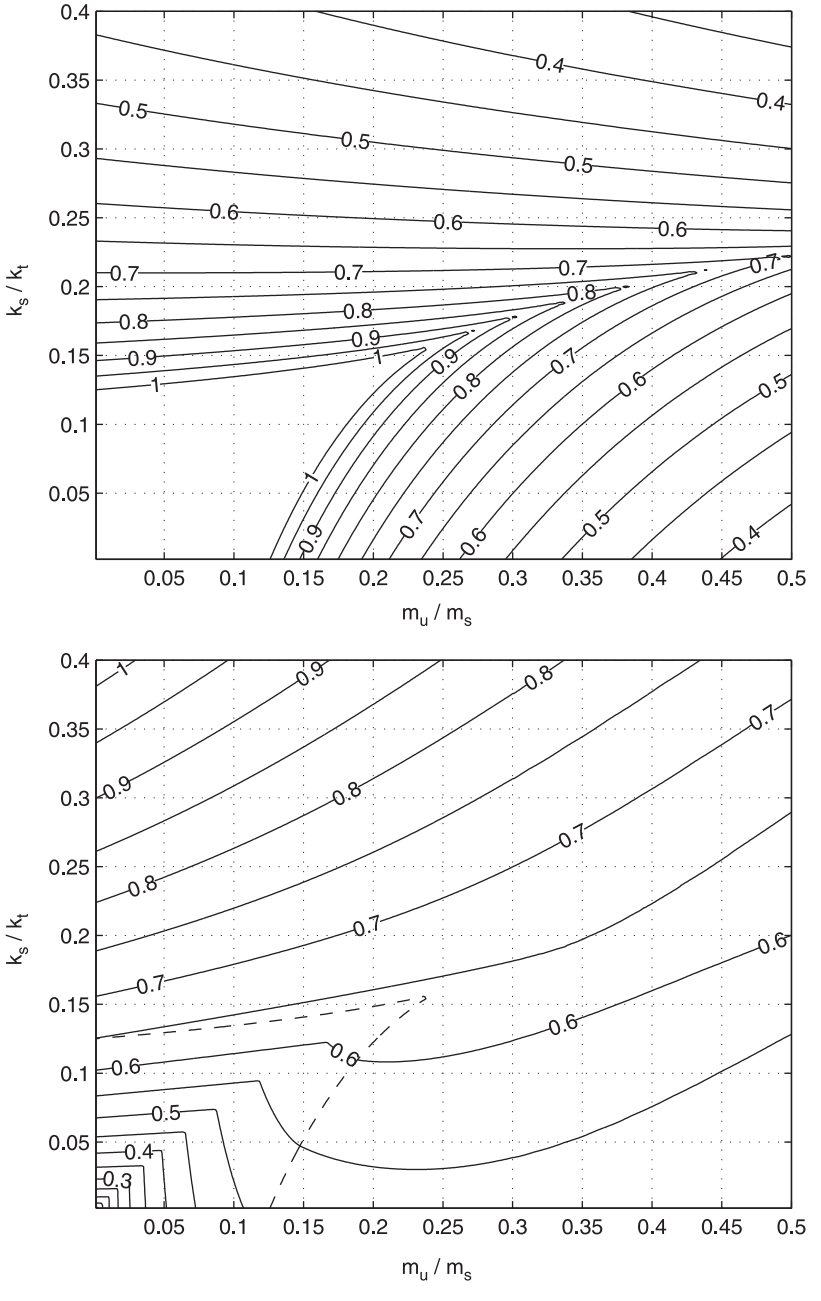

Figure A1. Contour plots of: (a) Optimal J_ϕ for S1, (b) Corresponding optimal normalised damping c.

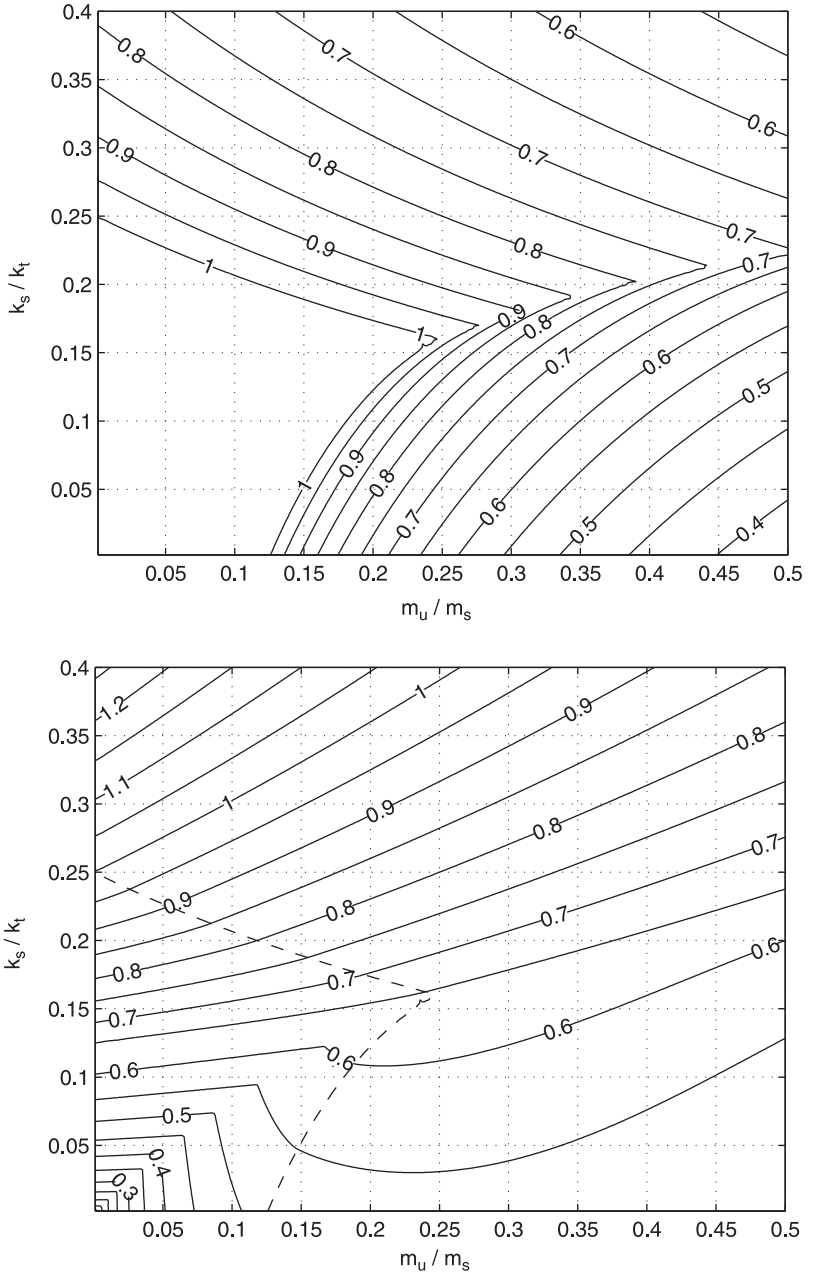

Figure A2. Contour plots of: (a) Optimal J_ϕ for S3, (b) Corresponding optimal normalised damping c.

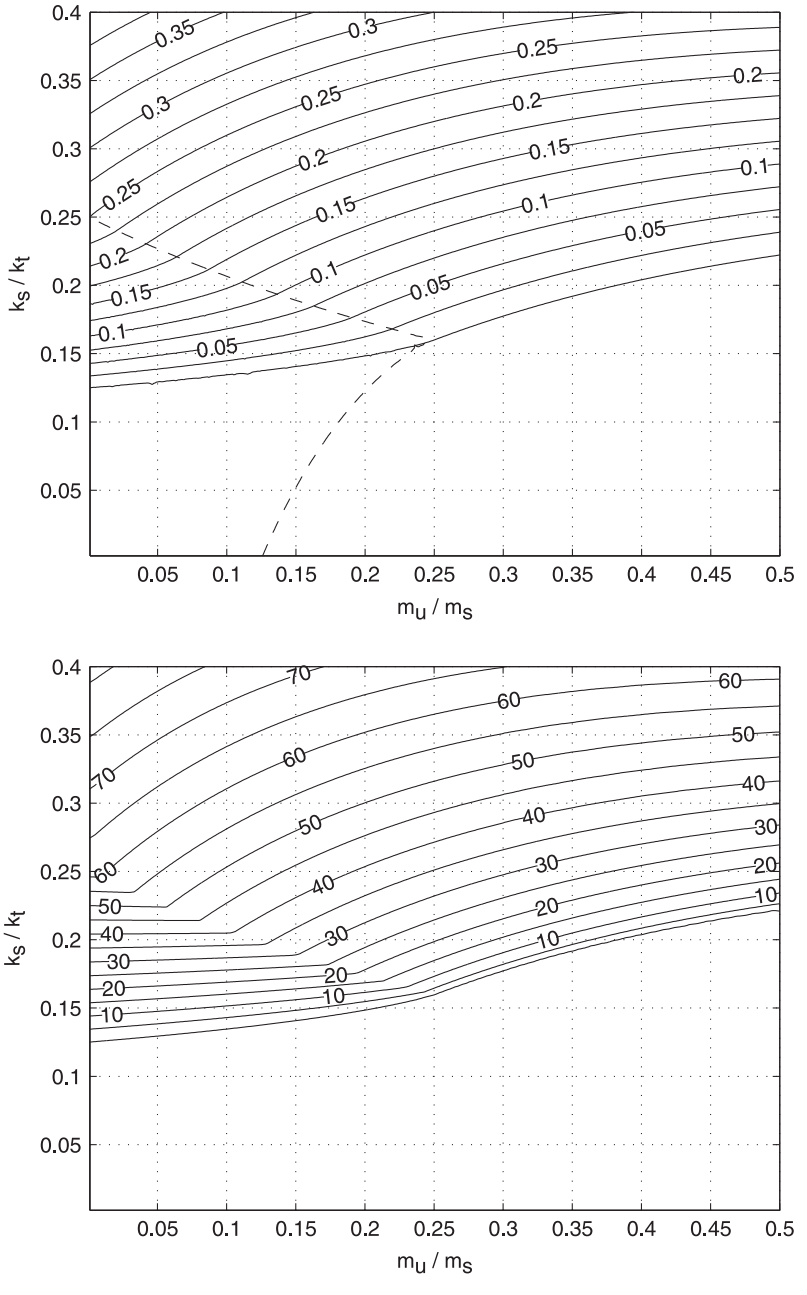

Figure A3. Contour plots of: (a) Optimal dimensionless inertance $\gamma = b/m_s$ for S3, (b) Percent improvement of S3 over S1.

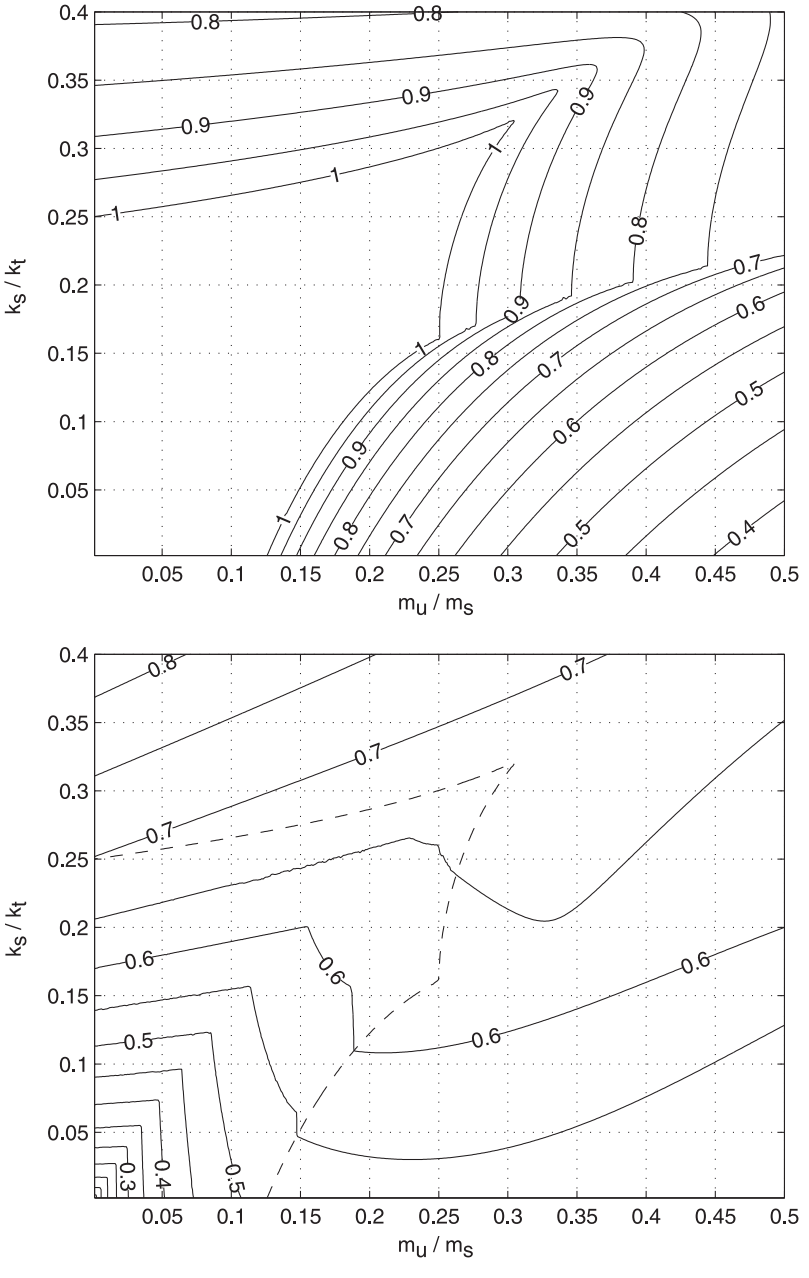

Figure A4. Contour plots of: (a) Optimal J_ϕ for S4, (b) Corresponding optimal normalised damping c.

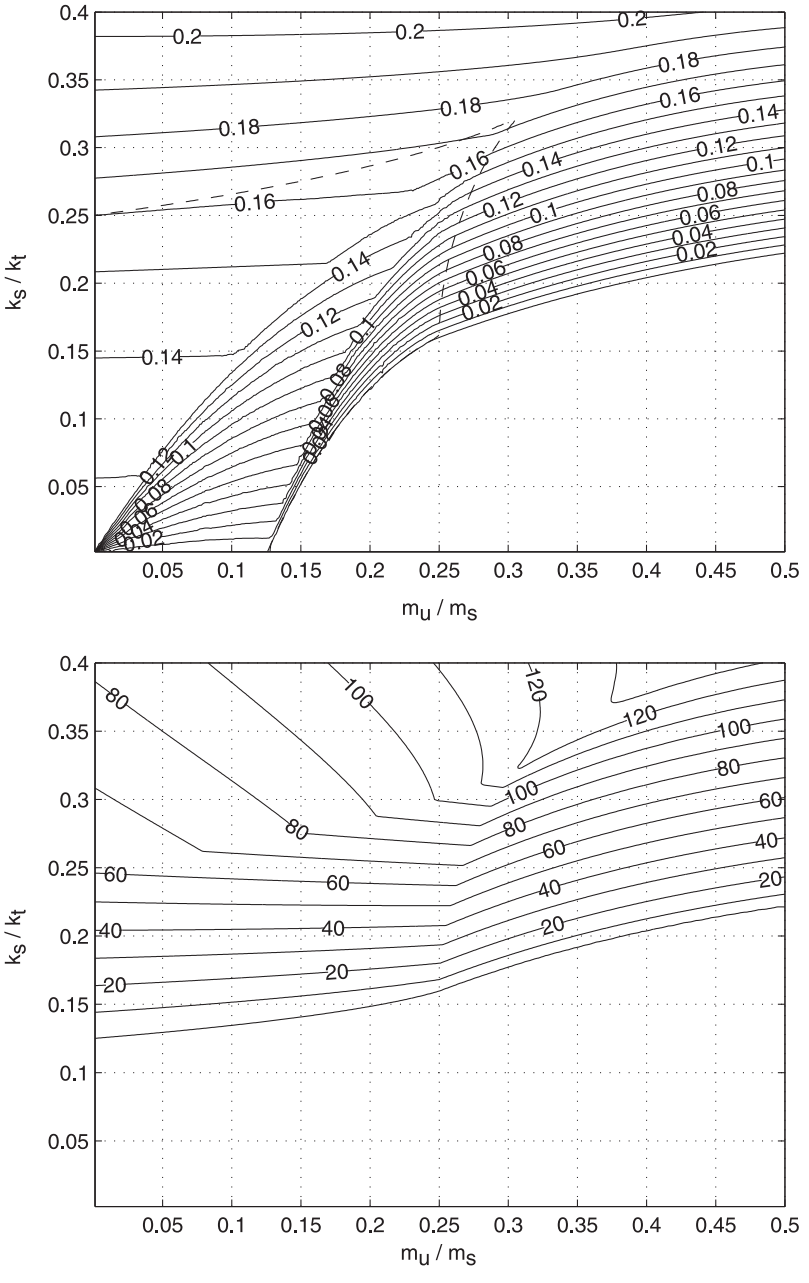

Figure A5. Contour plots of: (a) Reciprocal optimal dimensionless inertance $= \delta m_s/b$ for S4, (b) Percent improvement of S4 over S1.